
Article:
Rezaei Jegarluei, M orcid.org/0000-0002-6770-7161, Aristidou, P orcid.org/0000-0003-4429-0225, Fernandes, W et al. (1 more author) (2023) Wide-Area Backup Protection Using Sparse Synchronized/Unsynchronized PMU Measurements. IEEE Transactions on Power Delivery, 38 (4). pp. 2630-2640. ISSN 0885-8977

https://doi.org/10.1109/tpwrd.2023.3249822

Wide-Area Backup Protection Using Sparse Synchronized/Unsynchronized PMU Measurements

M. Rezaei Jegarluei, *Student Member*, *IEEE*, P. Aristidou, *Senior Member*, *IEEE*, W. Fernandes, and S. Azizi, *Senior Member, IEEE*

***Abstract*—This paper proposes a wide-area backup protection (WABP) method for transmission systems using sparse synchronized/unsynchronized PMU measurements. The method is aimed at addressing practical challenges such as temporary loss of the time-synchronization signal (LTSS), sparse PMU coverage, and communication failures and latencies. A linear and computationally efficient formulation is proposed to identify the faulted line in near real-time based on the superimposed-circuit concept. An index is proposed that quantifies the mismatch degrees between the expected and observed superimposed phasors without requiring full network observability. The method can work well with unsynchronized measurements without imposing a significant computational burden. This is achieved by canceling out the effect of angle drifts caused by LTSS from the equations. Since no matrix inversion is involved, sparse PMU measurements do not result in singularity, and thus, the unsolvability of the equations. A technique is proposed to assess the feasibility of faulted-line identification by a given set of PMUs. Being robust against measurement and parameter errors, the method performs well with PMUs of different reporting rates regardless of the fault distance, type, and resistance. More than 200,000 simulations conducted on the IEEE 39-bus test system verify the effectiveness of the proposed WABP method.**

***Index Terms*— Wide-area backup protection (WABP), phasor measurement unit (PMU), unsynchronized measurements, communication latencies.**

I. Introduction

PROTECTION systems play a crucial role in the secure operation of the power system in the face of faults [1]. For reasons such as logic/design deficiency, incorrect settings, and relay/communication failures, protection systems are prone to misoperation and malfunction. The hidden failure of local protection has been recognized as one of the main root causes of widespread disturbances [2]-[3]. Measurement errors caused by the transient behavior of instrument transformers also contribute to local protection failures [2]-[3]. Therefore, there has been a growing interest in alternative solutions over recent years to complement local protection schemes.

Wide-area backup protection (WABP) is defined as the processing of phasors provided by PMUs and other intelligent electronic devices to identify the faulted line and make appropriate commands [4]. This has great potential to enhance reliability as instrument transformers located farther from the fault location (FL) experience smaller voltage and current variations upon a fault [4]. To be practical, WABP must be able to make reliable decisions in near real-time. It must also be robust against the insufficiency of PMU data, various reporting rates of PMUs, communication failure and latencies, and the loss of the time-synchronization signal (LTSS).

PMU-based protection systems have been receiving more attention for implementation in practice in recent years, e.g., in Ecuador and India [5]. Great efforts have also been made in the literature to develop WABP methods to account for deficiencies of local backup protection [6]. In [7]-[8], the faulted line is identified by monitoring the operating statuses of circuit breakers and protective relays. However, these methods cannot serve the purpose of backup protection in the case of circuit breaker failures and relay maloperations. In [9], an effective WABP method is presented using the residual vector of a synchrophasor state estimator. However, subject to the PMU placement, this method might not be able to infer the presence or absence of a fault on some lines. The WABP methods presented in [10]-[17] also require the availability of PMUs at certain locations. Nevertheless, PMUs are normally installed considering financial constraints and the availability of communication infrastructure rather than the necessities of a specific functionality [18]. Even if all buses are equipped with PMUs, these methods might fail in the case of a PMU malfunction or partial communication failure. Existing wide-area fault location methods in [19]-[21] are not suitable for WABP due to technical difficulties attached to their nonlinear formulations and, thus, iterative solutions. These methods are computationally demanding and not flexible enough to deal with practical challenges. As they are essentially designed for offline calculations, the inherent attributes of these methods make them unsuitable for WABP.

A superimposed-circuit methodology is proposed in [22]-[25] to address practical challenges associated with WABP. A closed-form solution is derived by replacing the faulted line by two current sources based on the superposition theorem. However, these methods are vulnerable to temporary LTSS. Building upon the previous methods, [26] reformulates the system of equations as a linear combination of current sources and angle drifts caused by LTSS. In this formulation, the coefficient matrix relies on the measurements, and the outcome can be highly affected by erroneous measurements. Moreover, the solution of this system requires inversions and multiplications of large matrices, which make the formulation computationally inefficient for real-time applications.

Communication latency is a practical challenge faced by all real-time wide-area applications. Indeed, data associated with the same time instant from different PMUs are unlikely to be received simultaneously in the control center [27]. This calls

Mohammad Rezaei Jegarluei and Sadegh Azizi are with the School of Electronic and Electrical Engineering, University of Leeds, Leeds, LS2 9JT, UK (e-mail: elmrj@leeds.ac.uk; s.azizi@leeds.ac.uk).

Petros Aristidou is with the Department of Electrical Engineering, Computer Engineering and Informatics, Cyprus University of Technology, Limassol 3036, Cyprus (e-mail: p.aristidou@ieee.org).

William Fernandes is with Schweitzer Engineering Laboratories, Pullman, Washington, USA (e-mail: william_fernandes@selinc.com).

for defining a maximum wait time to make a decision based on the data received without having to wait for all data to arrive. Another technical difficulty, which is not addressed by the existing methods, is the possibility of having PMUs with different reporting rates. The proposed method accommodates sparse PMU coverage, PMU malfunction, and communication latencies/failures. This is because the method requires neither full network observability nor a fixed set of PMU data, which means a few delayed or missing PMU data can be tolerated.

This paper proposes a computationally efficient superimposed-circuit-based WABP method. An index is proposed to identify the faulted line by quantifying the mismatch degree between the observed and expected superimposed phasors. The proposed method works with measurements having different reporting rates and unsynchronized measurements without imposing a significant computational burden. It is robust against measurement and parameter errors and can identify the faulted line through a noniterative formulation regardless of the fault distance, type, and resistance. A simple yet effective technique is proposed to reduce the number of suspected lines as more PMU data is received in the control center. This is continued until only one line remains, i.e., the faulted line, or the wait time is reached.

The rest of this paper is organized as follows. Section II details the proposed methodology. Modifications applied to overcome practical challenges are presented in Section III. Section IV is devoted to the method's performance evaluation. Finally, concluding remarks are presented in Section V.

II. Proposed Wide-Area Backup Protection Method

In this section, a coefficient vector relating the voltage and current measurements to the fault current is derived using transfer impedances between measurements and the FL [9]. The transfer impedances are a nonlinear function of the FL, which is not known a priori. Solving this system of equations leads to the exact FL on the faulted line, which is time-consuming. This research focuses on identifying the faulted line rather than unnecessarily spending so much time to find the exact FL on the faulted line. This highly expedites the decision-making process and is similar to what local protection techniques, such as directional overcurrent, differential, and distance protection do to protect transmission lines [1]-[3]. To achieve this, the coefficient vectors at two fixed locations on each line are calculated offline. To identify the faulted line, an index is calculated for these locations. This whole process is ultra-fast yet quite reliable, as will be demonstrated in the simulation section.

A. System of Equations for WABP

Let us assume a fault has occurred at distance α on line *i*-*j* from bus *i*, as shown in Fig. 1(a). The fault type determines the interconnection of sequence circuits [1]. Nonetheless, each sequence circuit can be independently analyzed regardless of the fault type and resistance [24]. The superimposed circuit in sequence "*s*" is shown in Fig. 1(b). This circuit only includes one nodal current injection at FL, i.e., I_f^s, representing the fault current in that sequence circuit. This is because synchronous generators can be modeled as constant impedances in the superimposed circuit over the time frame of interest [1],[23]. The fault current path is entirely replaced by I_f^s. Thus, the fault resistance is not included in the bus impedance matrix. In this paper, the distributed parameter model of the line is used for modeling transmission lines.

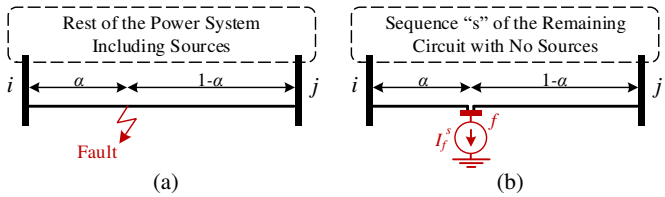

Fig. 1. (a) Whole faulted circuit. (b) Superimposed circuit representation.

Let $\boldsymbol{Z}^s$ denote the pre-fault bus impedance matrix of the sequence circuit "*s*" and bus f represent a virtual bus at the FL. The transfer impedance between a real bus, let us say bus u, and bus f can be obtained using entries of $\boldsymbol{Z}^s$, α, and the distributed parameters of line *i*-*j* by (1) shown at the bottom of this page [21], where l_{ij} and γ_{ij} denote the length and the propagation constant of the line, respectively. Based on the superimposed circuit representation during a fault on line *i*-*j* in Fig. 1(b), the superimposed voltage at an arbitrary bus u satisfies the following equation

$$\Delta V_u^s = Z_{u,f}^{T,s} I_f^s \tag{2}$$

where $Z_{u,f}^{T,s}$ is the transfer impedance between bus u and f in the sequence circuit "*s*", where superscript "*T*" is used to emphasize that $Z_{u,f}^{T,s}$ is different from the entries in the bus impedance matrix. The sending-end superimposed current of line *u*-*w*, denoted by ΔJ_{uw}, can be obtained from

$$\Delta J_{uw}^s = C_{uw,f} I_f^s \tag{3}$$

where the derivation of C_{uw} is detailed in [24].

Regarding available PMU measurements, all equations in the form of (2) and (3) together form an overdetermined system of equations as below

$$\boldsymbol{m}^{exp,s} = \boldsymbol{h}_f^s I_f^s \tag{4}$$

where $\boldsymbol{m}^{exp,s}$ represents the expected superimposed measurement vector induced by the fault current I_f^s, and $\boldsymbol{h}_f^s$ denotes the coefficient vector between PMU locations and bus f in the sequence circuit "*s*". Due to the time-invariant behavior of synchronous machines in the negative-sequence circuit and its higher accuracy than the zero-sequence circuit, the negative-sequence circuit is used for asymmetrical faults, while the positive-sequence circuit is utilized for symmetrical faults. The amounts of negative-sequence components are used to detect asymmetrical faults, as detailed in [26]. For simplicity, superscript "*s*" is dropped in the rest of the paper.

$$Z_{u,f}^{T,s} = \frac{\dfrac{Z_{i,u}^s}{\sinh\left(\gamma_{ij} l_{ij} \alpha\right)} + \dfrac{Z_{j,u}^s}{\sinh\left(\gamma_{ij} l_{ij} (1-\alpha)\right)}}{\dfrac{1}{\sinh\left(\gamma_{ij} l_{ij} \alpha\right)} + \dfrac{1}{\sinh\left(\gamma_{ij} l_{ij} (1-\alpha)\right)} + \tanh\left(\dfrac{\gamma_{ij} l_{ij}}{2} \alpha\right) + \tanh\left(\dfrac{\gamma_{ij} l_{ij}}{2} (1-\alpha)\right)} \tag{1}$$

B. Optimization Problem for Identifying the Faulted Line

In this paper, the nonlinearity regarding the exact fault distance on the faulted line is avoided using the coefficient vectors for a limited number of fixed *fault location candidates (FLCs)*. An index is calculated for every coefficient vector using the observed measurement vector. The index quantifies the *mismatch degree* (*MD*) between the expected and observed measurements, irrespective of the unknown fault current. Using this index, an optimization problem is formulated to identify the faulted line by finding the *FLC* whose coefficient vector has the smallest *MD*.

The following optimization problem can be solved to find the location of an event at which the expected measurement vector best matches the observed one.

$$event\ location = \underset{E \in \mathcal{E}}{\arg\min}(\|\boldsymbol{m} - \boldsymbol{m}^{exp,E}\|) \tag{5}$$

where $\boldsymbol{m}$ represents the observed measurement vector, and $\mathcal{E}$ denotes the set of possible events at different locations. Further, $\boldsymbol{m}^{exp,E}$ is the expected measurement vector for event E at a location. However, when $\mathcal{E}$ is restricted to a set of short circuit faults, (5) can be written as below by using (4) [28].

$$FLC^{*} = \underset{\forall\, FLC}{\arg\min}\left(\min_{I_f}\|\boldsymbol{m} - \boldsymbol{h}_{FLC}\, I_f\|\right) \tag{6}$$

where FLC^{*} represents the identified *FLC* which is the closest one to the actual FL. This optimization problem can be readily solved using dot products. Let us consider two vectors $\boldsymbol{a}$ and $\boldsymbol{b}$ with elements of complex numbers. From linear algebra, it is well-known that the projection of $\boldsymbol{a}$ onto $\boldsymbol{b}$, i.e., $proj_{\boldsymbol{b}}\boldsymbol{a}$, is the vector that minimizes $\|\boldsymbol{a} - \boldsymbol{b}k\|$, where k is a complex scalar [29]. The projection of $\boldsymbol{a}$ onto $\boldsymbol{b}$ can be obtained from

$$proj_{\boldsymbol{b}}\boldsymbol{a} = \underset{k}{\arg\min}\|\boldsymbol{a} - \boldsymbol{b}k\| = \left(\frac{\boldsymbol{a}\,.\boldsymbol{b}}{\boldsymbol{b}\,.\boldsymbol{b}}\right)^{*} \tag{7}$$

where $(\cdot)^{*}$ represents the conjugate operator. Using (7), the actual value of I_f in (6) can be disregarded. This is achieved by replacing I_f with a complex scalar obtained by (7) that results in the best match between the observed and expected measurements for every *FLC*. In other words, the complex scalar minimizes the objective function (6). This is advantageous because the fault current is an unknown variable in fault location formulations. Accordingly, the following index, which quantifies the minimum mismatch degree between the expected and observed phasors, is calculated regarding the coefficient vector of an *FLC*, i.e., $\boldsymbol{h}_{FLC}$.

$$MD_{\boldsymbol{m},\boldsymbol{h}_{FLC}} = \left\|\boldsymbol{m} - \boldsymbol{h}_{FLC}\left(\frac{\boldsymbol{m}\,.\boldsymbol{h}_{FLC}}{\boldsymbol{h}_{FLC}\,.\boldsymbol{h}_{FLC}}\right)^{*}\right\| \tag{8}$$

Using these indices, the problem (6) can be written as

$$FLC^{*} = \underset{\forall\, FLC}{\arg\min}\left(MD_{\boldsymbol{m},\boldsymbol{h}_{FLC}}\right) \tag{9}$$

Finally, the line associated with FLC^{*} is identified as the faulted line. It is worth noting that the *MD* calculated for an *FLC* that is exactly located at the true FL, i.e., virtual bus f, would be ideally zero if measurements were error-free.

C. Optimal Number and locations of FLCs

The closer the *FLC* is to the true FL, the closer lies the vector $\boldsymbol{h}_{FLC}$ to $\boldsymbol{h}_f$. If an *FLC* does not exactly locate at the FL,

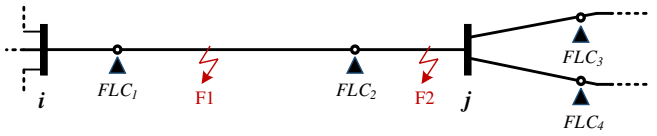

Fig. 2. Location of *FLC*s on transmission lines.

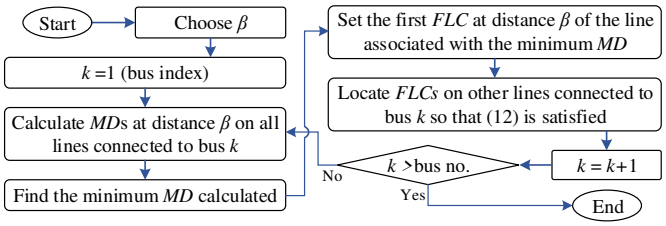

Fig. 3. Flowchart of the procedure for locating *FLC*s on all lines.

its corresponding coefficient vector, i.e., $\boldsymbol{h}_{FLC}$, deviates from the actual fault coefficient vector $\boldsymbol{h}_f$. This means that if an *FLC* is not exactly at the true FL, its corresponding *MD* will be larger. As the faulted line and the fault distance are not known in advance, a trivial approach is to consider many *FLC*s on every line in the set of candidates in (9) so that one of the *FLC*s is placed very close to the actual FL. This approach, however, would not be computationally efficient for protection applications, especially in large-scale power systems. More importantly, the proposed WABP method aims to identify the faulted line rather than the exact FL on it. As will be explained later, two *FLC*s at proper locations on every line would be sufficient, providing that the *MD* calculated for at least one of the *FLC*s on the faulted line is smaller than those for all other *FLC*s, irrespective of the fault distance.

The proposed approach for locating the *FLC*s on every line is presented here. As shown in Fig. 2, consider a fault, e.g., F1, between FLC_1 and FLC_2 on line *i*-*j*. This fault will be closer to either FLC_1 or FLC_2 than other *FLC*s at adjacent lines, regardless of their locations. As a result, the *MD* for FLC_1 or FLC_2 will be smaller than those for *FLC*s on the adjacent lines. Special considerations should be taken for a fault occurring within the end sections, i.e., between the FLC_2 and bus *j*. The *FLC*s around a common bus must be located so that their *MD*s for a fault at the common bus are equal. For example, the *FLC*s around bus *j* should be located so that

$$MD_{\boldsymbol{m}_j,\boldsymbol{h}_{FLC_2}} = MD_{\boldsymbol{m}_j,\boldsymbol{h}_{FLC_3}} = MD_{\boldsymbol{m}_j,\boldsymbol{h}_{FLC_4}} \tag{10}$$

where $\boldsymbol{m}_j$ is the measurement vector induced by an arbitrary fault at bus *j*. In doing so, a fault on an end section, e.g., F2 in Fig. 2, will be closer to the *FLC* on the faulted line, i.e., FLC_2. Thus, its corresponding *MD* will be smaller than *MD*s for *FLC*s on the adjacent lines, i.e., FLC_3 and FLC_4. Using (4), $\boldsymbol{m}_j$ can be written as $\boldsymbol{h}_j I_j$, in which I_j represents the fault current at bus *j*, and $\boldsymbol{h}_j$ is the coefficient vector at this bus. According to (8), it can be easily shown that

$$MD_{\boldsymbol{m}_j,\boldsymbol{h}_{FLC_k}} = |I_j| \cdot MD_{\boldsymbol{h}_j,\boldsymbol{h}_{FLC_k}} \tag{11}$$

where $|I_j|$ denotes the magnitude of the fault current at bus *j*. Regardless of $|I_j|$, (10) can be written as (12) using (11).

$$MD_{\boldsymbol{h}_j,\boldsymbol{h}_{FLC_2}} = MD_{\boldsymbol{h}_j,\boldsymbol{h}_{FLC_3}} = MD_{\boldsymbol{h}_j,\boldsymbol{h}_{FLC_4}} \tag{12}$$

To locate the *FLC*s around bus *j*, first, the *MD*s between $\boldsymbol{h}_j$ and the coefficient vectors at distance β from bus j are calculated for all lines connected to this bus. The location corresponding to the coefficient vector giving the smallest *MD* is taken as the first *FLC*. Without loss of generality, let us assume that FLC_2 is determined in this step. Then, FLC_3 and FLC_4 are located so that (12) holds true. This procedure should be done for all buses. As a result, an *FLC* is located at each opposite end of every line. Fig. 3 shows the flowchart of the process for locating *FLC*s across the system. This process will be further clarified using an example in subsection IV-B.

While the method does not place rigid limits on the value of β, it should be selected between 0 and 0.5 to ensure that one end section of any line does not overlap with its other end section. However, very small values for β result in locating the *FLC*s very close to the common buses, thereby having almost similar coefficient vectors. This might impact the method's performance in correctly identifying the faulted line because of possible measurement and parameter errors. The impact of β on the method's success rate on the IEEE 39-bus test system is scrutinized in subsection IV-A.

According to (12), all procedures for locating *FLC*s and calculating their coefficient vectors are conducted offline, thereby incurring no during-fault computational burden. Hence, the *MD* indices for every *FLC* using (8) can be quickly computed in near real-time. The proposed method proves to be faster than existing methods. A detailed analysis of the computational burden of the proposed method and the most recent existing method is presented in subsection IV-D.

III. Considerations for Practical Challenges

Wide-area methods are subject to bad data caused by device failures or cyber-attacks. The robustness against cyber-attacks can be enhanced using reliable encryption protocols. Moreover, the proposed indices are calculated based on the well-known least-squares method [29]. This allows for bad data detection approaches, e.g., the largest normalized residual test [30]. As the calculation of *MD*s is not dependent on any specific measurements, removing the equations associated with bad data will not render the formulation unsolvable.

The WABP formulation put forward in the previous section assumes that PMU data are all available. However, this assumption may not hold true in practice for different reasons, such as LTSS, sparse PMU coverage, communication failure, communication latencies, and having PMUs with different reporting rates. This section embeds effective solutions in the method to ensure the success of WABP in the face of the challenges mentioned. In addition, the fault detection criteria and the interaction logic between the proposed method and the primary protection systems are detailed.

A. Loss of the Time-Synchronization Signal (LTSS)

Unpredictable factors such as GPS antenna failure, atmospheric disturbances, electromagnetic interference, and cyberattacks may occasionally cause LTSS [31]. However, (8) can be utilized to calculate *MD*s with synchronized measurements only. Following an LTSS, the phase-angles of observed phasors will become unreliable. Nevertheless, unsynchronized measurements can still be incorporated into the WABP formulations by only considering their magnitudes. In doing so, the following index will be formed based only on the magnitudes of measurements as *MD* of magnitudes.

$$MD^{mag}_{\boldsymbol{m},\boldsymbol{h}_{FLC}} = \left\| |\boldsymbol{m}| - |\boldsymbol{h}_{FLC}| \cdot \frac{|\boldsymbol{m}|.|\boldsymbol{h}_{FLC}|}{|\boldsymbol{h}_{FLC}|.|\boldsymbol{h}_{FLC}|} \right\| \qquad (13)$$

where the operator $|\cdot|$ extracts the magnitudes of the elements in a vector. Although the phase angles are not accurate with respect to each other following an LTSS, those provided by PMUs at a substation always remain aligned with respect to the same local time reference [32]. This means there is still useful information in the measurements that can be exploited.

At each bus, a GPS server receives GPS signals as a source to generate the time synchronization signal. In the event of the loss of the GPS signal, the GPS server continues distributing time signals for the PMUs at that bus using an internal clock [33]. This could introduce a time drift from the accurate time signal of the GPS, which can become unacceptably large if the GPS signal is not restored. However, with or without the GPS signal, the time references for measurements associated with a bus remain the same [11], [32]. Accordingly, to model the impact of LTSS, phase-angles reported by PMUs at buses 1 to *Np* are added by unknown angle drifts, θ_1^{LTSS}, …, $\theta_{Np}^{\text{LTSS}}$, respectively. In other words, if the observed measurement vector is sorted as $\boldsymbol{m} = [\boldsymbol{m}_1, \dots, \boldsymbol{m}_p, \dots, \boldsymbol{m}_{Np}]$, in which $\boldsymbol{m}_p$ includes measurements associated with bus *p*, we have

$$\angle \boldsymbol{m}_p = \angle \boldsymbol{m}_p^{exp} + \vec{\mathbf{1}} \cdot \theta_p^{\text{LTSS}} \quad , \quad 1 \le \text{p} \le Np \qquad (14)$$

where the operator $\angle$ extracts the phase-angle of the elements in a vector. The vector $\boldsymbol{m}_p^{exp}$ stands for the expected PMU measurements at bus *p*, and $\vec{\mathbf{1}}$ denotes a vector of ones. The vector $\boldsymbol{h}_f$ can also be sorted as $\boldsymbol{h}_f = [\boldsymbol{h}_{f,1}, \dots, \boldsymbol{h}_{f,p}, \dots, \boldsymbol{h}_{f,Np}]$, where the vector $\boldsymbol{h}_{f,p}$ includes the elements of $\boldsymbol{h}_f$ that are associated with phasors reported by PMUs at bus *p*. As per (4), $\angle \boldsymbol{m}_p^{exp} = \angle \boldsymbol{h}_{f,p} + \vec{\mathbf{1}} \cdot \angle I_f$. Thus, (14) can be written as

$$\angle \boldsymbol{m}_p - \angle \boldsymbol{h}_{f,p} = \vec{\mathbf{1}} \cdot \left(\angle I_f + \theta_p^{\text{LTSS}} \right) \quad , \quad 1 \le \text{p} \le Np \qquad (15)$$

The right side of (15) is a vector with identical elements for phasors associated with the same bus. Variance is a measure of the dispersion of samples in a data set from their mean. It is defined as the average of the squared deviations from the mean. It can be easily confirmed that the vector on the right side of (15) has a zero variance, ideally. Based on this property, the following index can be calculated as *MD* of angles for every *FLC*s regardless of the phase angle of the fault current, $\angle I_f$, and LTSS angle drifts.

$$MD^{ang}_{\boldsymbol{m},\boldsymbol{h}_{FLC}} = \sum_{p=1}^{Np} Var\ (\angle \boldsymbol{m}_p - \angle \boldsymbol{h}_{FLC,p}) \qquad (16)$$

Finally, the total mismatch degree is obtained using the normalized *MD*s of magnitudes and angles, i.e., $\overline{MD^{mag}_{\boldsymbol{m},\boldsymbol{h}_{FLC}}}$ and $\overline{MD^{ang}_{\boldsymbol{m},\boldsymbol{h}_{FLC}}}$. To normalize *MD*s at any time instant, these are divided by the maximum of the *MD*s calculated for that time instant. The share of $\overline{MD^{mag}_{\boldsymbol{m},\boldsymbol{h}_{FLC}}}$ and $\overline{MD^{ang}_{\boldsymbol{m},\boldsymbol{h}_{FLC}}}$ in the total *MD* can be set by two coefficients, $\mathcal{W}_1$ and $\mathcal{W}_2$, as follows

$$MD_{\boldsymbol{m},\boldsymbol{h}_{FLC}} = \mathcal{W}_1 \cdot \overline{MD^{mag}_{\boldsymbol{m},\boldsymbol{h}_{FLC}}} + \mathcal{W}_2 \cdot \overline{MD^{ang}_{\boldsymbol{m},\boldsymbol{h}_{FLC}}} \qquad (17)$$

Since the faulted line is identified with the minimum MD, dividing all MDs by the same scalar does not affect the results for the faulted-line identification. Thus, (17) can be reformulated as below by dividing both sides by $\mathcal{W}_2$.

$$MD_{\boldsymbol{m},\boldsymbol{h}_{FLC}} = W \cdot \overline{MD^{mag}_{\boldsymbol{m},\boldsymbol{h}_{FLC}}} + \overline{MD^{ang}_{\boldsymbol{m},\boldsymbol{h}_{FLC}}} \tag{18}$$

To investigate the impact of W on the success rate of the method, a sensitivity analysis is presented in subsection IV-A.

B. Sparse PMU Coverage

Full network observability is not a prerequisite for the proposed method. Theoretically, the method could identify the faulted line using two PMU data at different locations, providing that the coefficient vectors for the *FLC*s on the faulted line are linearly independent of those on other lines. This is because the fault current can take any value that results in the least mismatch degree between the observed and expected measurements, as in (6) and (7). From linear algebra [29], the normalized dot product of two linearly dependent vectors is 1. Based upon this fact, an index quantifying the mutual *dependence degree* (DD) between different coefficient vectors, namely $\boldsymbol{h}_{FLC_u}$ and $\boldsymbol{h}_{FLC_w}$, can be obtained as

$$DD_{FLC_u,FLC_w} = \left| \frac{\boldsymbol{h}_{FLC_u}}{\|\boldsymbol{h}_{FLC_u}\|} \cdot \frac{\boldsymbol{h}_{FLC_w}}{\|\boldsymbol{h}_{FLC_w}\|} \right| \tag{19}$$

To account for rounding and parameter errors, it is better to define a security threshold for DD, e.g., 0.99, to confirm mutual dependency. Following a fault, the coefficient vectors with a DD of 1 will have the same MD with respect to the observed measurement vector. Therefore, if their MD is smaller than all other candidates, it would not be possible to distinguish the true faulted line between them. However, according to (8) and (9), the faulted line can be distinctly identified, provided that the coefficient vectors of the faulted line and those of other lines are not mutually dependent.

Unlike existing residual-based methods [23]-[26], sparse PMU measurements would never cause unsolvability and singularity issues. This is because there is no matrix inversion in the proposed formulation. Furthermore, all coefficient vectors and their mutual DDs can be readily computed offline using the bus impedance matrix and the selected locations for *FLC*s. Hence, prior to the fault onset in a power system with sparse PMU measurements, we know which lines can be uniquely identified if faulted. The lines corresponding to coefficient vectors with mutual DDs of 1 will all be identified as suspected lines if a fault occurs on any of them.

C. Communication Latency

As stated in IEEE standard C37.118.2 [27], communication latencies may vary from a few milliseconds to even seconds for many reasons, such as routing, forwarding, error checking, equipment malfunctions, communication infrastructure limits, and cyber-attacks [34]. The unpredictable behavior of communication latencies makes it a major challenge to wide-area applications [31]. Hence, WABP should not be dependent on the availability of a fixed set of PMUs as their data might get lost or not received in the action time of WABP. This is not a problem with the proposed method, as it does not place rigid limits on the number and locations of PMUs. Indeed,

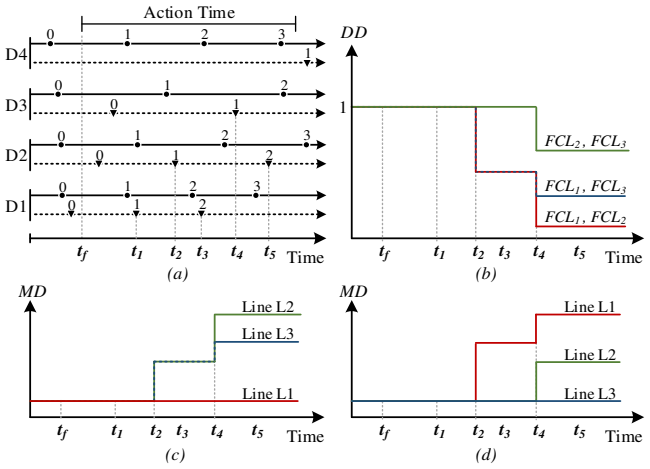

Fig. 4. (a) Timelines of time-tags and receiving time instant. (b) Mutual DDs between coefficient vectors. (c). Calculated DDs following a fault on line L1. (d) Calculated DDs following a fault on line L3.

removing the equations associated with missing/delayed PMU data will not render the WABP formulation unsolvable unless the remaining data are linearly dependent, which is rarely the case. Nevertheless, this might lead to having mutually dependent coefficient vectors, as the dimension of coefficient vectors is determined by the number of PMU data received.

The maximum number of PMU data lost that can be tolerated by the method to distinctly identify the faulted line depends on the faulted line and the locations of PMUs whose data has been successfully collected. For any combinations of received PMU data, however, all DDs between different coefficient vectors can be computed offline by (19). Thus, for any scenario of loss of PMU data, the system operator would know which lines can be distinctly identified and which lines have the same MD if a fault occurs on any of them.

In the desired action time for WABP, the superimposed circuit in Fig. 1 remains valid. One phasor reported before and one after the fault onset would be enough to obtain the superimposed quantities employed in the system of equations (4) [26]. Thus, the method can run properly with PMUs having different reporting rates. The method can function correctly irrespective of the exact time instant at which the phasors have been measured and time-tagged as long as they are within the timeframe of interest for the WABP.

Fig. 4 illustrates the performance of the proposed method in the presence of communication latencies, which will be further verified by simulations in subsection IV-E. Timelines of time tags and reception time instants of four data, denoted by D1 to D4, with different reporting rates, are shown in Fig. 4(a). The solid timeline represents the sampling time instant at which the corresponding data are time-tagged by a PMU, while the dashed one shows the time instant at which the data are received at the control center. Each measured sample and its corresponding received data are numbered by a superscript from 0 onwards. Fig. 4(b) shows the assumed mutual DDs between coefficient vectors for FLC_1, FLC_2, and FLC_3 on lines L1, L2, and L3, respectively, over time. Assuming that a fault occurs at $t=t_f$, the first post-fault sample $D1^1$ is received at $t=t_1$. However, as per (19), coefficient vectors with merely one element are always linearly dependent, which means they will have a DD of 1 until $t=t_2$, at which the sample $D2^1$ is

received. As explained, all previous samples of other data received in the action time can be utilized together with new samples in the proposed superimposed-based formulation.

Having received $D2^1$, the dimensions of coefficient vectors become two. In this condition, the coefficient vectors of FLC_2 and FLC_3 are assumed to be linearly dependent, whereas FLC_1 is assumed independent of the formers. That is why $DD_{FLC2,FLC3}$ is 1, and $DD_{FLC1,FLC2}$ and $DD_{FLC1,FLC3}$ are less than 1 after $t=t_2$ until the reception of new data at $t=t_4$. Next, the data sample $D3^1$ is received at $t=t_4$. Consequently, the dimension of coefficient vectors increases to three. Now, they all are assumed to be mutually independent, which is why all mutual DDs become less than 1 from $t=t_4$ onwards. In this example, data D4 is not received during the desired action time because of communication failure, so it is not used in the WABP formulation. It is worth noting that at $t=t_3$ and $t=t_5$, the values of D1 and D2 are updated by $D1^2$ and $D2^2$, respectively. This, however, does not affect the dimension of the coefficient vectors and the values of DDs, but it helps to update MDs regarding minor variations of post-fault phasors.

For the scenario described for mutual DDs between coefficient vectors, the resulting MDs for a fault on lines L1 and L3 will be as shown in Fig. 4(c) and 4(d), respectively. Until $t=t_2$ in both cases, the MDs are the same and remain the minimum because all coefficient vectors are mutually dependent. As can be seen in Fig. 4(c), for a fault on line L1, the MDs of L2 and L3 increase and depart from that of L1 after $t=t_2$. Hence, the faulted line can be discriminately identified from other candidates following $t=t_2$ using only data D1 and D2.

As shown in Fig. 4(d), for a fault on lines L3 (or L2) between time $t=t_2$ and $t=t_4$, line L1 is excluded from the suspected lines, thus having both L2 and L3 suspected. Although the faulted line is not distinctly identified, the shortage of input data between $t=t_2$ and $t=t_4$ will not render the WABP formulations unsolvable. Instead, valuable information can be derived from the received data to limit the number of suspected lines. Subsequently, more lines can be excluded from the suspected lines by receiving new data. This approach is continued in the action time until only one line remains in the set of suspected lines, e.g., time t_4 following the fault onset on L3 in this example. Hence, the faulted line can be correctly identified before the reception of all data, e.g., data D4.

D. Fault Detection and Interaction with Primary Protection

As detailed in subsection IV-D, the computation time of the method is in the order of a few milliseconds. Therefore, the method can continuously run in the control center to calculate mismatch degrees of magnitudes (MD^{mag}) of all lines using (13). In normal conditions, the superimposed quantities and, thus, all MD^{mag}s are negligible. After a short circuit fault, mismatch degrees of non-faulted lines move away from zero, while that of the faulted line remains negligible. A fault is detected once both criteria below are met:

- The maximum MD^{mag} is bigger than a threshold.
- The ratio between the maximum and the minimum MD^{mag} exceeds another threshold.

In this paper, these thresholds are 1 and 5, respectively. One should not use mismatch degrees of phase-angles (MD^{ang}) for fault detection because angles of the negligible superimposed quantities during normal conditions are unreliable.

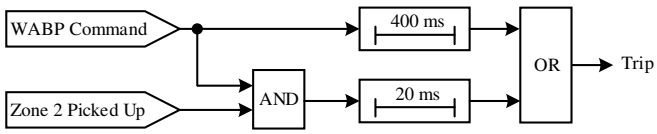

Fig. 5. Tripping logic of the proposed method.

Due to indefinite communication latencies [27], wide-area protection methods are not typically aimed at providing primary protection but backup protection. However, owing to the low computation burden, the proposed method can be employed in the primary protection system if the latency of the system-wide communications is limited to tens of milliseconds. Receiving an overriding signal from the control center can be extremely helpful in reducing the intentional time delays applied to guarantee the coordination between relays and/or to ensure the fault is within the intended reach.

The main aim of WABP methods is to come into effect in case the primary protection has failed to operate. Thus, a few hundred milliseconds are available to ensure sufficient PMU data have been received at the control center. The time setting of the method for acting as stand-alone backup protection can be the same as that of the local backup protection relays, e.g., 300-500 ms for transmission level [1]-[2]. This time delay ensures that sufficient PMU data has been delivered to the control center so that the WABP method can decisively pinpoint the faulted line. It should be noted that the WABP command is only sent to the identified faulted line. As a result, the WABP does not take action on the healthy lines.

Fig. 5 shows the tripping logic incorporating the command generated by the proposed method into the primary protection. In this logic, the WABP commands are used as a permissive signal for permissive overreaching transfer trip protection [2]-[3]. Following the reception of a WABP command at a line terminal, the line's circuit breaker is tripped after 20 ms, provided that the primary distance relay is correctly operating and has picked up in its zone 2. This allows for fast fault clearance over 100% of the line length. Moreover, in case of failure/misoperation of the local relay, the method will act as stand-alone backup protection by tripping the circuit breaker after 400 ms from the fault onset.

IV. Performance Evaluation

The performance of the proposed method is evaluated by conducting more than 200,000 simulations on the IEEE 39-bus test system with 34 lines. First, the general performance of the proposed method is evaluated for various fault types/resistance at different locations with synchronized and unsynchronized measurements. Next, the sensitivity of the method to inaccuracies in line/generator parameters and measurement errors is scrutinized. Then, the computational burden of the method is compared with that of the most recent method. Finally, the method's performance in the face of communication latencies and sparse PMU coverage is studied.

DIgSILENT PowerFactory is the software utilized for obtaining time-domain voltage and current waveforms. These waveforms are first filtered by an anti-aliasing Butterworth filter with a cut-off frequency of 400 Hz and then sampled

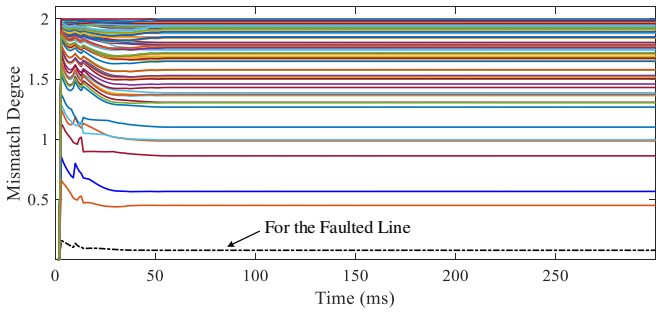

Fig. 6. Mismatch degrees following a 1-ph-g fault at 20% of line 21-22.

TABLE I
SUCCESS RATE (%) OF THE PROPOSED WABP METHOD

Fault Type	Synchronized meas.				Unsynchronized meas.			
	0 Ω	20 Ω	50 Ω	100 Ω	0 Ω	20 Ω	50 Ω	100 Ω
Symmetrical	99.74	99.69	99.52	99.31	99.18	99.07	98.92	98.75
Asymmetrical	99.68	99.54	99.26	99.07	99.51	99.34	99.11	98.98

with frequency 2 kHz. Finally, the phasors are extracted using the Discrete Fourier Transform (DFT). If higher accuracy is desired, more effective phasor extraction methods, e.g., the complete PMU model in [35], could be used.

To consider compliance specifications of PMUs, magnitude and angle error bounds are combined into a single quantity known as total vector error (TVE) [27]. The TVE measures the difference between the true phasor and the reported one. The IEEE standard for synchrophasor measurements establishes a criterion of 1% for the TVE [27]. Thus, PMU data are manipulated to have a random TVE between 0% and 1% in all conducted simulations. In doing so, a TVE with an evenly distributed random magnitude between 0% and 1% and a random angle between 0 and 2π is applied to all phasors. The performance of the proposed method for measurements with higher TVEs is studied in subsection IV-C.

A. General Evaluation of the Proposed Method

The proposed WABP method is first examined through a few arbitrarily selected examples. Buses 3, 5, 8, 11, 14, 16, 19, 23, 25, 27, 29, and 39 are equipped with PMUs. Fig. 6 shows the normalized MDs for all FLCs for up to 300 ms after a solid 1-ph-g fault at 20% of line 21-22, where FLCs are located with the ratio β of 0.1. The coefficient W in (18) is chosen at 1. As can be seen, The MD corresponding to the FLC on the faulted line closer to the actual FL is the smallest with sufficient distinction among that of other lines.

The general performance of the proposed method is examined through various fault types at 20 evenly distributed distances on every line with fault resistances of 0 Ω, 20 Ω, 50 Ω, and 100 Ω. Table I reports the success rate of the proposed method in identifying the faulted line with synchronized and unsynchronized measurements at 60 ms following the fault onset ignoring communication latencies. In this study, β and W are set at 0.1 and 1, respectively. The method's sensitivity to β and W will also be studied in this subsection. To make measurements unsynchronized, the angles of the phasors associated with each PMU are all added with a random angle drift between 0 and 2π. It can be seen from Table I that the method is highly successful in faulted line identification irrespective of the fault distance, type, and resistance.

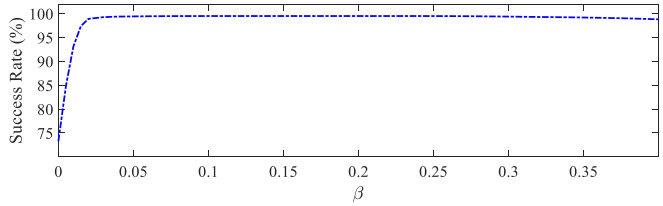

Fig. 7. Sensitivity of the proposed method to the value of β.

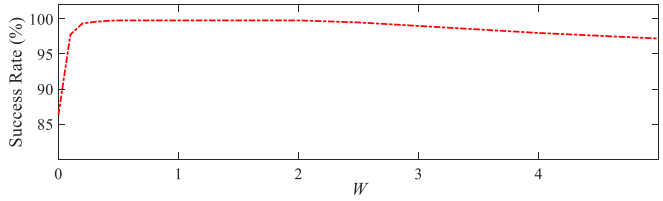

Fig. 8. Sensitivity of the proposed method to the value of W.

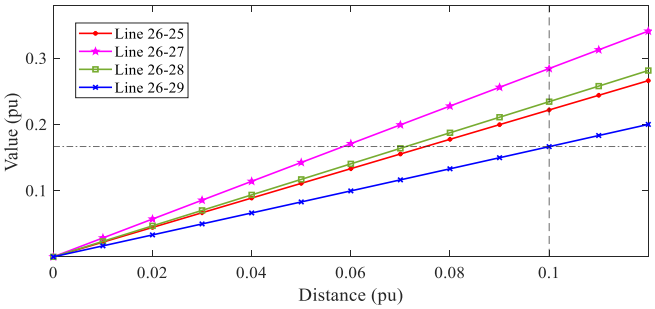

Fig. 9. Mismatch degree between the coefficient vector at bus 26 and the coefficient vectors at distance 0 to 0.12 pu on all lines connected to bus 26.

Simulations show that the method is rarely unsuccessful for a few faults very close to a bus in areas with poor PMU coverage. Following a fault very close to a bus without a PMU, the difference between the MDs calculated for the FLCs around that bus could be quite small. Therefore, measurement/ parameter errors might lead to wrong identification of the faulted line. Specifically, the proposed method only failed for a few fault cases at distance 2% of lines 7-8 and 26-27.

As mentioned, the location of FLCs is determined by the ratio β. In this study, the sensitivity of the method to β is scrutinized. Fig. 7 shows the success rate of the proposed method with different values of β for all fault cases studied in Table I, while the weighting coefficient W is set at 1. As can be seen, the method is not noticeably impacted by β in the range [0.03, 0.4]. However, too small and very large values for β could impair the performance of the method.

The sensitivity of the method with unsynchronized measurements to W is also scrutinized. Fig. 8 shows the success rate for different values of W, with β set at 0.1. As can be seen, the success rate of the proposed method is more than 99% for W between 0.3 and 2. The success rate drops to 86% if MDs are calculated with either $\overline{MD^{mag}}$ or $\overline{MD^{ang}}$ only by setting $W \gg 1$ and $W = 0$ in (18), respectively.

B. Procedure for Locating FLCs

The procedure for locating FLCs around bus 26 is detailed here. Fig. 9 shows the MDs between the coefficient vector at bus 26 and the coefficient vectors at distances 0 to 0.12 pu on all lines connected to this bus. Let us assume β is set at 0.1.

TABLE II
WABP SENSITIVITY TO MEASUREMENT AND PARAMETER ERRORS

Type of Error	Error Range (%)				
	±1	±2	±3	±4	±5
With Measurement Err.	99.55%	99.40%	99.34%	99.11%	98.75%
With Parameter Err.	99.36%	99.18%	99.07%	98.72%	98.33%

TABLE III
COMPUTATION TIME OF THE PROPOSED AND EXISTING METHODS

Meas. Type	Synchronized meas.		Unsynchronized meas.	
References	[26]	Prop.	[26]	Prop.
48 measurements 34 lines	20 ms	<1 ms	50 ms	<1 ms
1000 measurements 200 lines	150 ms	6 ms	8400 ms	10 ms

TABLE IV
TIME-TAGS AND DELIVERY TIME INSTANT AT CONTROL CENTER

PMU's bus	3	8, 11	19	16	25, 29	14, 23	27	5, 39
Time-tag	40 ms	45 ms	55 ms	60 ms	70 ms	75 ms	85 ms	90 ms
Delivery	60 ms		80 ms		100 ms		120 ms	

The location at distance 0.1 on line 26-29 that gives the smallest *MD* is taken as the first *FLC*. Then, other *FLC*s on lines 26-25, 26-27, and 26-28 are located at distances 0.075, 0.058, and 0.071 on the respective lines so that they have the same *MD* as the selected *FLC* on line 26-29 to satisfy (12).

C. Sensitivity to Measurement and Parameter Errors

This subsection studies the impact of measurement and parameter errors on the performance of the proposed method. To this end, 100 arbitrary faults are applied across the power system. For reporting success rates in Table II, each fault case is repeated 1,000 times for every error range with evenly distributed random errors. The method functions correctly for more than 98.75% and 98.33% of the cases with up to 5% errors in measurements and parameters, respectively. The method proves to be quite robust against measurement and parameter errors. However, excessive errors in the bus impedance matrix can impair its performance. According to the GB Grid Code, the minimum dependability index of protection systems must be 99%. As reported in Table II, the method is more than 99% successful with reasonable input errors. For example, in IEEE standard C37.118.1, the TVE of PMU measurements is mandated to be less than 1% [27]. In this paper, however, larger input errors are only investigated to demonstrate the robustness of the proposed WABP method against excessive measurement/parameter errors.

D. Computational Burden

As detailed in Appendix, the total time needed for calculating all mismatch degrees is

$$T_{total} < 18N_L N_m(T_{mul} + T_{sum}) \tag{20}$$

where N_L and N_m denote the number of transmission lines and measurements, and T_{mul} and T_{sum} are the time needed for a multiplication and summation operation, respectively. It is worth noting that the computation time refers to the time needed to make a decision after receiving the PMU data at the control center and does not account for communication latencies. The existing wide-area fault location methods, such as [19]-[21], use computationally expensive nonlinear and iterative approaches for fault location. The most recent WABP method presented by the authors in [26] utilizes a noniterative closed-form linear formulation for WABP. That method is, however, computationally demanding compared to the proposed method, especially with unsynchronized measurements. This is because of several transpositions, multiplications, and inversions operations on large matrices in the real-time operation during faults included in [26]. The computation times of the proposed method and [26] with synchronized and unsynchronized measurements for two different power systems are reported in Table III. In this study, a personal computer with a 2.8 GHz processor and 8 GB of RAM is employed. As can be seen, due to the huge computation time, the method [26] would not be advantageous for large power systems with unsynchronized measurements.

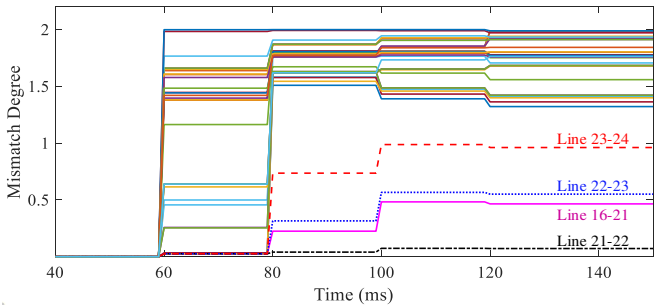

Fig. 10. Calculated mismatch degrees following a 1-ph-g fault at 20% of line 21-22 considering communication latencies listed in Table IV.

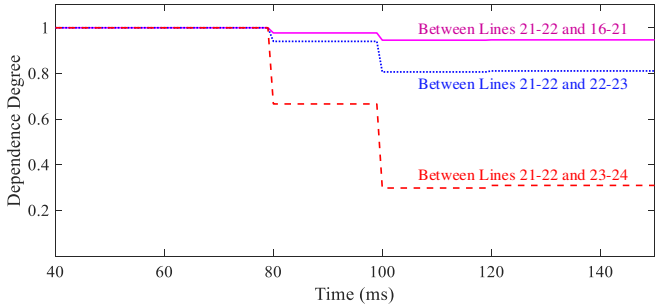

Fig. 11. Dependence degrees between the faulted line 21-22 and lines 16-21, 22-23, and 23-24 with communication latencies listed in Table IV.

E. Sparse PMU Coverage and Communication Latencies

As described earlier, the proposed method does not require full network observability or specific PMU placements. Therefore, missing PMU data could be well tolerated. Having said this, however, delayed/missing PMU data or sparse PMU coverage might result in having some *FLC*s with linearly dependent coefficient vectors. As a result, lines with mutually dependent coefficient vectors will be all suspected if a fault occurs on any of them. Even so, the proposed method can identify the faulted line or limit the number of suspected lines based on partially received PMU data. The set of suspected lines may be refined after receiving more data.

To demonstrate the above point, different communication latencies are assumed for every PMU. To make matters worse, it is assumed that only one post-fault phasor sample is

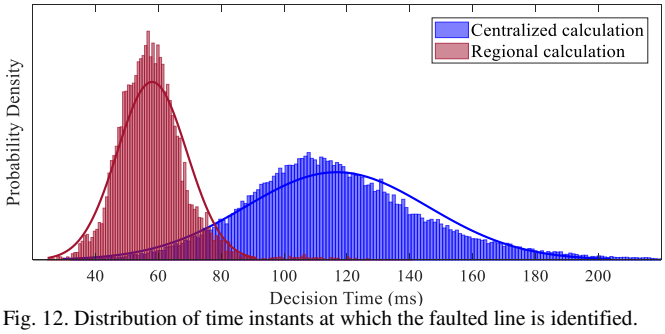

Fig. 12. Distribution of time instants at which the faulted line is identified.

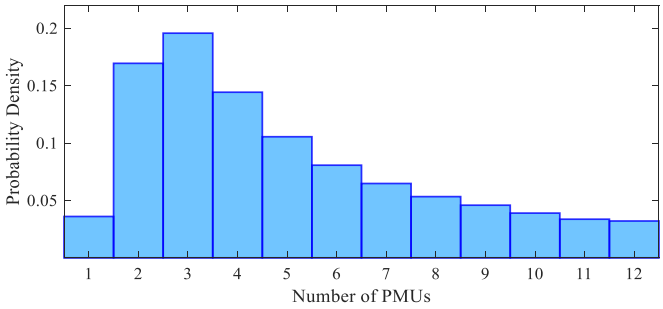

Fig. 13. Distribution of the number of PMUs whose data are received at the control center once the faulted line is distinctly identified.

delivered to the control center from each PMU. Table IV lists the time instant after the fault onset at which PMU data are time-tagged and received at the control center. Fig. 10 depicts the *MD*s of all sending-side *FLC*s following a solid 1-ph-g fault at 20% of line 21-22 for up to 150 ms. It can be observed that between 60 ms and 80 ms following the fault onset, the *MD*s belonging to lines 21-22, 22-23, 23-24, and 21-16 are identical and less than all other *MD*s. This means that after collecting data from only three PMUs, the number of suspected lines reduces from 34 to 4. The suspected lines are updated by receiving new data so that between 80 ms and 100 ms, the *MD*s corresponding to non-faulted lines rise, while the *MD* of the *FLC* on the faulted line 21-22 remains the smallest. As a result, line 21-22 is identified as the faulted line using only five PMUs at buses 3, 8, 11, 16, and 19. As shown in Fig. 11, the trend of *MD*s can also be verified by the trend of mutual *DD*s. The mutual *DD*s between coefficient vectors of line 21-22 and adjacent lines are all 1 between 60 ms and 80 ms, thereby having the same *MD*s over this period. From 80 ms onwards, the mutual *DD*s drop below 1, resulting in discriminative *MD*s to identify the faulted line.

A comprehensive performance evaluation in the face of communication latencies is conducted here. As described, the calculation of the proposed *MD*s is not dependent on specific measurements. Hence, the method can also be utilized in regional control centers by using only regional measurements as long as the bus impedance matrix is available at these centers. Effective methods such as [36] can be used for accurately estimating the parameters of power system components. These parameters can be utilized to calculate the bus impedance matrix based on the network topology, as detailed in [37]. According to the formulation put forward, the bus impedance matrix of the whole network model is used for the regional implementation of the method. However, the network model can be efficiently limited to a smaller area whose boundaries are observed by PMUs. This technique has recently been proposed and successfully tested in [24].

TABLE V
PERFORMANCE OF THE PROPOSED WABP IN THE PRESENCE OF RENEWABLES

Fault Type	IBR Penetration Level (%)				
	10	20	40	60	80
Symmetrical	99.13%	98.75%	97.66%	96.13%	94.43%
Asymmetrical	99.17%	99.01 %	98.16%	97.27%	96.11%

To evaluate the method's performance with regional-based calculations versus the centralized large area-based calculations, the test system has been divided into three regions with respect to its geographical characteristics, as in [24]. The proposed method in each regional control center is assumed to only use data from PMUs installed in that region. Communication latencies can be reduced by dividing a large area into small regions. Thus, in the simulations conducted, communication latencies between PMUs in each region and their associated regional control center are assumed to be smaller than those between PMUs and the central large-area control center. Accordingly, regional communication latencies are assumed to have normal distributions with mean 40 ms and standard deviation 10 ms, whereas these for large-area communication are 100 ms and 30 ms, respectively [38].

The same set of 100 arbitrary faults used in subsection IV-C is applied. In order to obtain solid results, each fault case is repeated 1,000 times considering random communication latencies for every 12 PMUs. Fig. 12 shows the distributions of decision time instants after the fault onset with centralized and regional calculations (in the Western region). The average decision time by the method with centralized calculation is around 115 ms after the fault onset. Although the regional center only uses 6 PMUs, the average decision time is reduced to 61 ms because of smaller communication latencies within the region. The distribution of the number of PMUs whose data are received before making a decisive decision with centralized calculations is shown in Fig. 13. The average number of PMUs used to make the final decision is only 5. More importantly, these are not predetermined PMUs but those whose data have been received early enough.

F. Sensitivity to the Presence of Renewables

The presence of renewables has not been addressed by the proposed method. However, due to their smaller fault current contributions compared to those from synchronous generators, low penetration of renewables does not noticeably impair the method's performance. The method's sensitivity to different penetration levels of renewables is studied by adding 20 wind turbines with the same nominal powers at buses 1, 3, 4, 5, 7, 8, 9, 11, 12, 13, 14, 15, 16, 17, 18, 21, 24, 26, 27, and 28. To model different penetration levels, the nominal powers of renewables are modified based on the desired penetration level. The total active power generation in the system is maintained constant by reducing the synchronous generation. Renewables are assumed to have low-voltage ride-through capabilities defined in the GB Gird Codes. Table V reports the method's success rate for different fault types across the system in the presence of renewables with various penetration levels. As expected, high penetration of renewables slightly reduces the success rate of the proposed method.

TABLE A-I
THE COMPUTATION BURDEN OF EVERY MISMATCH DEGREE

Equation	Operation	No. of Mul.	No. of Sum.
(13)	$x1 = \|\boldsymbol{m}\|.\|\boldsymbol{h}\|$	N_m	N_m
	$x2 = \|\boldsymbol{h}\|.\|\boldsymbol{h}\|$	N_m	N_m
	$\boldsymbol{x3} = \|\boldsymbol{h}\|\ (x1 \div x2)$	N_m+1	0
	$MD^{mag} = \|\ \|\boldsymbol{m}\| - \boldsymbol{x3}\ \|$	N_m	$2N_m$
(16)	$\boldsymbol{y1} = \angle\boldsymbol{m} - \angle\boldsymbol{h}$	0	N_m
	$y2 = mean(\angle\boldsymbol{m} - \angle\boldsymbol{h})$	N_p	N_m
	$MD^{ang} = \left\|\boldsymbol{y1} - \vec{\boldsymbol{1}} \cdot y2\right\|^2$	N_m	$2N_m$
(18)	Norm. MD^{mag} and MD^{ang}	$2N_m$	0
	$MD = W \cdot \overline{MD^{mag}} + \overline{MD^{ang}}$	N_m	N_m
Total		$8N_m + N_p + 1$	$9N_m$

V. CONCLUSION

This paper puts forward a wide-area backup protection method by sparse synchronized/unsynchronized phasor measurements. A computationally efficient formulation is developed to identify the faulted line by quantifying the mismatch degree between the expected and observed superimposed phasors. The impact of unknown angle drifts caused by a temporary loss of the time-synchronization signal is canceled out from the formulations. This remarkably reduces the computational burden induced to cope with unsynchronized measurements compared to the existing methods. Extensive simulation studies conducted confirm that the method performs well in the presence of communication latencies/failures with PMUs of different reporting rates.

The method is robust against measurement/parameter errors and can quickly identify the faulted line regardless of the fault distance, type, and resistance. The linearity and simplicity of the derived formulations remove concerns over convergence speed and help to overcome practical challenges such as sparse PMU coverage and communication latencies/failures. Moreover, since no matrix inversion is involved, sparse PMU measurements do not result in unsolvability and singularity issues. These features are beyond the capability of the existing WABP methods. An index is introduced to determine whether the faulted line can be uniquely identified with any sets of PMU data received. Thanks to the robustness against practical challenges, low-demanding nature, and low data requirements, the proposed method has great potential for employment in practical real-time applications. Improvements to the proposed method for considering the presence of renewables and bad data would be proper directions for future research on WABP.

APPENDIX: ANALYSIS OF COMPUTATION BURDEN

All coefficient vectors are computed offline, with no impact on the real-time computational burden of the proposed method. Table A-I details the step-by-step number of summation and multiplication operations needed for obtaining the MD of a coefficient vector, in which N_m and N_p denote the number of measurements and PMUs, respectively. In the last row of the table, since N_m is bigger than $N_p + 1$ in power systems, $N_p + 1$ is replaced by N_m. As a result, the total time needed for calculating all MDs, i.e., T_{total}, is constrained as

$$T_{total} < 9N_m(T_{mul} + T_{sum}) \times N_{FLC} \qquad \text{(A-1)}$$

where N_{FLC} is the number of coefficient vectors, and T_{mul} and T_{sum} are the time needed for conducting a multiplication and summation operation, respectively. As described in Section II-D, the proposed method requires only two *FLC*s on every transmission line. Therefore, the total computation time of all MDs can be obtained by replacing N_{FLC} in (A-1) by $2N_L$, where N_L represents the number of transmission lines.

REFERENCES

[1] S. H. Horowitz and A. G. Phadke, *Power System Relaying*, 4th ed. John Wiley & Sons, 2008.

[2] J. L. Blackburn and T. J. Domin, *Protective Relaying: Principles and Applications*. Florida, USA: CRC Press, 2014.

[3] G. Ziegler, *Numerical Distance Protection: Principles and Applications*, 4th ed., Bavaria, Germany: Publicis Corporate Publishing, 2011.

[4] V. Terzija *et al.*, "Wide-area monitoring, protection, and control of future electric power networks," *Proc. IEEE*, vol. 99, no. 1, pp. 80–93, 2011.

[5] C. Halliday, *Visualization of real-time system dynamics using enhanced monitoring (VISOR)*, SP Energy Network, 2018.

[6] M. R. Jegarluei, J. S. Cortes, S. Azizi, and V. Terzija, "Wide-area event identification in power systems: A review of the state-of-the-art," 2022 *Int. Conf. Smart Grid Synch. Meas. and Analytics*, 2022, pp. 1–7.

[7] X. Tong *et al.*, "The study of a regional decentralized peer-to-peer negotiation-based wide-area backup protection multi-agent system," *IEEE Trans. Smart Grid*, vol. 4, no. 2, pp. 1197–1206, Jun. 2013.

[8] M. Chen, H. Wang, S. Shen, and B. He, "Research on a distance relay-based wide-area backup protection algorithm for transmission lines," *IEEE Trans. Power Del.*, vol. 32, no. 1, pp. 97–105, Feb. 2017.

[9] P. V. Navalkar and S. A. Soman, "Secure remote backup protection of transmission lines using synchrophasors, " *IEEE Trans. Power Del.*, vol. 26, no. 1, pp. 87-96, Jan. 2011.

[10] P. Kundu, A. K. Pradhan, "Synchrophasor-assisted zone-3 operation." *IEEE Trans. Power Syst.*, vol. 29, no. 2, pp. 660–667, Apr. 2014.

[11] J. Ma, C. Liu, and J. S. Thorp, "A wide-area backup protection algorithm based on distance protection fitting factor," *IEEE Trans. Power Del.*, vol. 31, no. 5, pp. 2196–2205, Oct. 2016.

[12] S. Gajare, J. G. Rao, O. D. Naidu, AK. Pradhan, "Wide-area measurement system-based supervision of protection schemes with minimum number of phasor measurement units, " *Phil. Trans. Roy. Soc. A*, vol 375, no. 2100, 2017.

[13] J. Ma et al., "A fault steady-state component-based wide-area backup protection algorithm," *IEEE Trans. Smart Grid*, vol. 2, no. 3, pp. 468–475, Sep. 2011.

[14] M. K. Neyestanaki and A. M. Ranjbar, "An adaptive PMU-based wide area backup protection scheme for power transmission lines," *IEEE Trans. Smart Grid*, vol. 6, no. 3, pp. 1550–1559, May 2015.

[15] M. M. Eissa, M. E. Masoud, and M. M. M. Elanwar, "A novel back up wide area protection technique for power transmission grids using phasor measurement unit," *IEEE Trans. Power Del.*, vol. 25, no. 1, pp. 270-278, Jan. 2010.

[16] Z. He, Z. Zhang, W. Chen, O. P. Malik, and X. Yin, "Wide-area backup protection algorithm based on fault component voltage distribution," *IEEE Trans. Power Del.*, vol. 26, no. 4, pp. 2752-2760, Oct. 2011.

[17] J. Zare, F. Aminifar and M. Sanaye-Pasand, "Synchrophasor-based wide-area backup protection scheme with data requirement analysis," *IEEE Trans. Power Del.*, vol. 30, no. 3, pp. 1410-1419, June 2015.

[18] Z. H. Rather *et al.*, "Realistic approach for phasor measurement unit placement: Consideration of practical hidden costs," *IEEE Trans. Power Del.*, vol. 30, no. 1, pp. 3–15, Feb. 2015.

[19] Q. Jiang, X. Li, B. Wang, and H. Wang, "PMU-based fault location using voltage measurements in large transmission networks," *IEEE Trans. Power Del*., vol. 27, no. 3, pp. 1644–1652, Jul. 2012.

[20] N. Kang and Y. Liao, "Double-circuit transmission-line fault location with the availability of limited voltage measurements," *IEEE Trans. Power Del.*, vol. 27, no. 1, pp. 325–336, 2012.

[21] A. S. Dobakhshari, "Fast accurate fault location on transmission system utilizing wide-area unsynchronized measurements," *Int. J. Electr. Power Energy Syst.*, vol. 101, pp. 234–242, Oct. 2018.

[22] M. R. Jegarluei, A. S. Dobakhshari, and S. Azizi, "Reducing the computational complexity of wide-area backup protection in power systems," *IEEE Trans. Power Del.*, vol. 37, no. 3, pp. 2421–2424, 2022.

[23] S. Azizi and M. Sanaye-Pasand, "A straightforward method for wide-area fault location on transmission networks," *IEEE Trans. Power Del*., vol. 30, no. 1, pp. 441–445, Feb. 2015.
[24] S. Azizi and M. Sanaye-Pasand, "From available synchrophasor data to short-circuit fault identity: Formulation and feasibility analysis," *IEEE Trans. Power Sys*t., vol. 32, no. 3, pp. 2062-2071, May 2017.
[25] M. R. Jegarluei, T. E. H. El-Gorashi, J. M. H. Elmirghani, and S. Azizi, "A generalized closed-from solution for wide-area fault location by characterizing the distributions of superimposed errors," *IEEE Trans. on Power Del.,* vol. 37, no. 6, pp. 5484-5487, 2022.
[26] S. Azizi, G. Liu, A. S. Dobakhshari, and V. Terzija, "Wide-area backup protection against asymmetrical faults using available phasor measurements," *IEEE Trans. Power Del*., Dec 2019.
[27] *IEEE Standard for Synchrophasor Measurements for Power Systems, IEEE Std. C37.118.1-2011, 2011.*
[28] J. E. Tate, and T. J. Overbye, "Line outage detection using phasor angle measurements," *IEEE Trans. Power Syst.*, vol. 23, no. 4, pp. 1644–1652, Nov. 2008.
[29] H. Anton*, Elementary Linear Algebra*, 8th ed. New York: Wiley, 2000, pp. 303–312.
[30] A. Abur and A. G. Exposito, *Power System State Estimation: Theory and Implementation*, Marcel Dekker, Inc., 2004.
[31] G. Feng, A. Abur, "Fault location using wide-area measurements and sparse estimation," *IEEE Trans. Power Syst*. Vol. 31, no. 4, pp. 2938–2945, Jul. 2016.
[32] W. Yao et al., "Impact of GPS signal loss and its mitigation in power system synchronized measurement devices," *IEEE Trans. Smart Grid*, vol. 9, no. 2, pp. 1141–1149, Mar. 2016.
[33] R. Das et al., "Distribution automation strategies: evolution of technologies and the business case," *IEEE Trans. Smart Grid*, vol. 6, no. 4, pp. 2166-2175, July 2015.
[34] C. Huang *et al.*, "A bounded model of the communication delay for system integrity protection schemes," *IEEE Trans. Power Del.*, vol. 31, no. 4, pp. 1921–1933, Aug. 2016.
[35] P. Romano, and M. Paolone, "Enhanced interpolated-DFT for synchrophasor estimation in FPGAs: Theory, implementation, and validation of a PMU prototype," *IEEE Trans. Instrum. Meas*., vol. 63, no. 12, pp. 2824–2836, Dec. 2014.
[36] A. S. Dobakhshari, M. Abdolmaleki, V. Terzija, and S. Azizi, "Online noniterative estimation of transmission line and transformer parameters by SCADA data," *IEEE Trans. on Power Syst.*, vol. 36, no. 3, pp. 2632-2641, May 2021.
[37] J. J. Grainger and W. D. Stevenson, *Power System Analysis*. New York, NY, USA: McGraw-Hill, 1999.
[38] M. Chenine and L. Nordström, "Investigation of communication delays and data incompleteness in multi-PMU wide area monitoring and control systems," *Proc. Int. Conf. Elect. Power Energy Convers. Syst. (EPECS)*, Sharjah, UAE, pp. 1–6, Nov. 2009.